# Measuring protein-membrane interaction through radial fluorescence correlation in 2 dimensions

# Measuring protein-membrane interaction through radial fluorescence correlation in 2 dimensions

N. Philipp,[1,2] E. Gratton,[3] and L. C. Estrada[1,2,*]

[1] *Universidad de Buenos Aires, Facultad de Ciencias Exactas y Naturales, Departamento de Física. Buenos Aires, Argentina*
[2] *CONICET - Universidad de Buenos Aires, Instituto de Física de Buenos Aires (IFIBA). Buenos Aires, Argentina*
[3] *Department of Biomedical Engineering, University of California, Irvine, USA*
[*] *lestrada@df.uba.ar*

**Keywords:** spectroscopy, fluorescence imaging, protein dynamics

**Abstract:** The cell membrane has a fundamental role in the cell life cycle but there's still much to be learned about its heterogeneous structure, regulation, and protein interaction. Additionally, the protein-membrane interaction is often overlooked when studying specific protein dynamics. In this work, we present a new tool for a better understanding of protein dynamics and membrane function using live cells and fast non-invasive techniques without the need for individual particle tracking. To this end, we used the 2D-pair correlation function (2D-pCF) to study protein interactions across cellular membranes. We performed numerical simulations and confocal experiments using a GAP-mEGFP fusion construct known to interact with the plasmatic membrane. Our results demonstrate that based on a quantitative correlation analysis as the 2D pair correlation of the signal intensities, is possible to characterize protein-membrane interactions in live systems and real-time. Combining experimental and numerical results this work presents a new powerful approach to the study of the dynamic protein-membrane interaction.

## 1. Introduction

The molecular flow at the subcellular level is a key element in regulating cell functions. This regulation depends on the physical structure of the surrounding cellular components, molecular interactions, and protein transport. In turn, these depend on multiple parameters such as the molecular species, the aggregations' states, and the cell life cycle [1–5]. The plasma membrane (PM) forms a 3D maze for proteins to reach their active sites. It has many functions and is fundamental for communication with the environment and other cells. Among these functions, the PM regulates cell growth, shape, movement, and division [6, 7].

Besides the PM, other important membranes that constitute the cell include the nuclear envelope (NE) and the endoplasmic reticulum (ER) membrane. Each of those has a crucial role in regulating and protecting their overall functionality. Membranes must therefore be selectively permeable to allow molecular exchange via carrier or channel proteins embedded within the membrane. In addition, because transport may sometimes be required in opposition to a gradient of concentration, many processes require active transport mechanisms that effectively pump required molecules across a membrane. The presence of membranes, while fundamental for cell function, also represents an obstacle to molecular free diffusion. The possibility of visualizing and understanding the path followed by molecules while crossing those membranes could unveil new aspects of their roles [3, 8–10]. Since membranes are continuously remodeling, the opportunity to visualize the transport across membranes requires a high spatio-temporal resolution analysis. It is with this objective that Digman and coworkers [11] first described the pair correlation approach (pCF) as a tool to map the molecular paths to diffusion inside the cell. A decade after the pair correlation approach pioneering work the bi-dimensional version, the 2D-pCF, was also developed in Gratton's lab [12].

The high resolution of 2D-pCF requires image acquisition with high time resolution combined

with increased sensitivity to measure the intensity fluctuations due to fast-moving molecules. This must be joined by a large field of view to see the whole cell. Afterward, for the performance of the pCF analysis, an efficient algorithm is needed due to the enormous amount of correlation functions that must be calculated across all pixels and all times of the measurement.

Thus the pair correlation function approach allows the measurement of obstacles (such as membranes) to the diffusion of proteins. In this work, we present an application of this method to address a specific problem, the measurement of the interaction strength (IS) between protein and membranes as a tool for a better understanding of protein dynamics and membrane functions.

## 2. Methods

### 2.1. Simulations

To first validate our proposed methodology we performed simulations using the commercial software SimFCS (LFD, UCI, www.lfd.uci.edu). We simulated molecules (proteins) with a brightness of 100,000 counts per second per molecule (cpsm) freely diffusing in a 128x128 pixels box (1 pixel = 50 nm). The pixel dwell time for the scanning was set at 10 $\mu$s/px and the box was illuminated by a laser beam moving in a raster-scan fashion. The frame time was 0.16 s and the simulation had a total of 4,000 frames.

A handwritten mask of a 2 pixels width (schematically representing a membrane) was placed at the center of the simulated box. The simulation requires the specification of additional parameters such as the diffusion coefficient (from 1 to 40 $\mu m^2$/s outside the mask and 1 to 1000 times slower inside) and the concentration of molecules (from 2 to 48 molecules/$\mu m^2$), as well as the probability to cross the mask ($0 \leq p \leq 1$). We will compare impenetrable barriers ($p = 0$) and penetrable barriers ($p > 0$).

### 2.2. 2D Pair Correlation Function

Fluorescence Correlation Spectroscopies (FCS) is a well-known family of microscopy approaches that provide information about the dynamics of fluorescently labeled molecules from the intensity fluctuations encoded in the emitted signal. It provides information at the single molecule level by averaging the behavior of many molecules and thus yields very good statistics. At the same time, they are minimally invasive techniques, allowing the study of the behavior of single proteins in live intact cells [11, 13–15].

The pair correlation method is a spatio-temporal correlation-based approach that correlates in space and time fluorescence signal fluctuations. Particularly, the pair correlation function (pCF) detects molecular transport by computing the cross-correlation of intensity fluctuations arising from the same molecules for all pairs of points in a scanned line mapping the molecular flow with a resolution given by the microscope's point spread function (PSF) [11]. When a pair of points are located further apart than two times the size of the PSF, there is a maximum in the correlation curve which appears at the average time it takes a molecule to move between the two locations. If the region where the molecular transport takes place is spatially homogeneous and the diffusion isotropic, the average time to travel a given distance is independent of the specific direction (blue molecules in Figure 1a). On the contrary, if an obstacle to molecular mobility appears during molecular diffusion, and molecules must overcome the obstacle, the average time to reach the same distance will be longer (red molecules in Figure 1a). Finally, if there is an impenetrable obstacle, the correlation between the two locations will be null, and the pCF curve zero, meaning that the molecule will never connect those locations (green molecules in Figure 1 a). The pCF is defined as in Eq. 1:

$$pCF(r_1 - r_0, \tau) = \frac{\langle F(r_0, t) \cdot F(r_1, t + \tau) \rangle}{\langle F(r_0, t) \cdot F(r_1, t) \rangle} \quad (1)$$

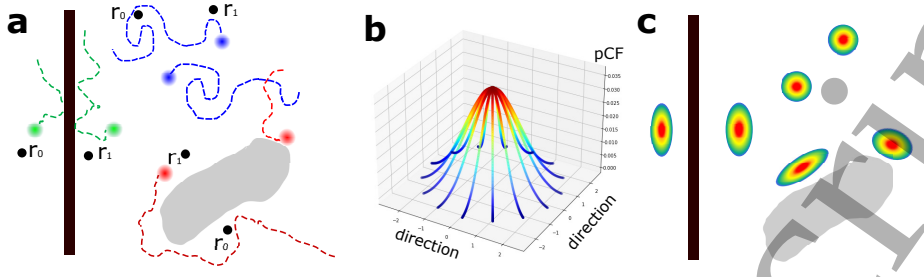


Fig. 1. **The pair correlation function concept. The SPRITE shape is an indicator of the presence of a barrier to diffusion**. (a) schematic representation of three possible diffusion cases: isotropic diffusion in free space (blue molecules), anisotropic diffusion due to the presence of an object (red), and anisotropic diffusion due to an impenetrable barrier (green). (b) Symmetrical SPRITE of an isotropic diffusion. (c) 2D representation of the sprite of anisotropy for each pixel in the scenario presented in (a).

where F is the fluorescence intensity at positions $r_0$ and $r_1$, and time $t$, $\tau$ is the time delay between acquisitions, and the temporal average is represented with brackets.

The spatio-temporal correlation function can be calculated at different distances and a maximum of the correlation function will appear at the average time a molecule takes to move between the two points. The pCF over a line has been successfully used to determine molecular transport in a broad range of diverse applications by our lab [16–18] and others [19–22]. In the 2D version of the technique [12], for each pixel, $r_0$, in the image, the pCF is calculated at every angle equally spaced around a circle of radius R pixels and centered at $r_0$ defining the temporal pCF curve at a distance of R pixels pCF(R). The resulting pCF curves are represented in a polar plot by radially arranging the correlation functions (Figure 1(b)). This polar plot is usually called a SPRITE and can be computed at each pixel of the image. In a system where molecules diffuse isotropically, the SPRITE would have a 3D symmetrical shape. If there is any diffusion barrier, the SPRITE will be distorted having an ellipse shape as schematically shown in Figure 1(c) for the molecules in Figure 1(a). We will use the distortion of the SPRITE as an indicator of the presence of barriers to diffusion and thus, to define the anisotropy as in Eq. 2:

$$A = \frac{\lambda_{long} - \lambda_{short}}{\lambda_{long} + \lambda_{short}} \tag{2}$$

where $\lambda$ is the radius of the long and short axis of the SPRITE.

Once we have calculated the anisotropy in each pixel we can create the anisotropy map to visualize the average dynamics of the molecules as the direction of the long axis of the SPRITE in each pixel. Only those pixels with an anisotropy higher than the average will be shown. Figure 2 shows simulations where molecules undergo (a) isotropic diffusion in a free space (b) isotropic diffusion in the presence of an impenetrable barrier (c) isotropic diffusion on both sides of an impenetrable barrier (d) and in the presence of a permeable barrier with a 2 pixels width.

The 2D-pCF anisotropy map allows us to differentiate each case apart from the intensity map. In the first case (i) there isn't any preferential direction while there is an obvious one in (j-l). In the latter, a gap forms between the two rows of high vertical anisotropy. We can measure the gap between those two lines by looking at the anisotropy profile (last row in Figure 2). When there is a preferential direction for diffusion, there is also a high anisotropy value. In the case of a barrier to diffusion, for a pCF(4) we see only one peak in the anisotropy profile (Figure 2 (n) and (o)). In the case of (p), where the molecules have the chance of diffusing inside the thin mask that slows them down, we have two peaks in the profile.

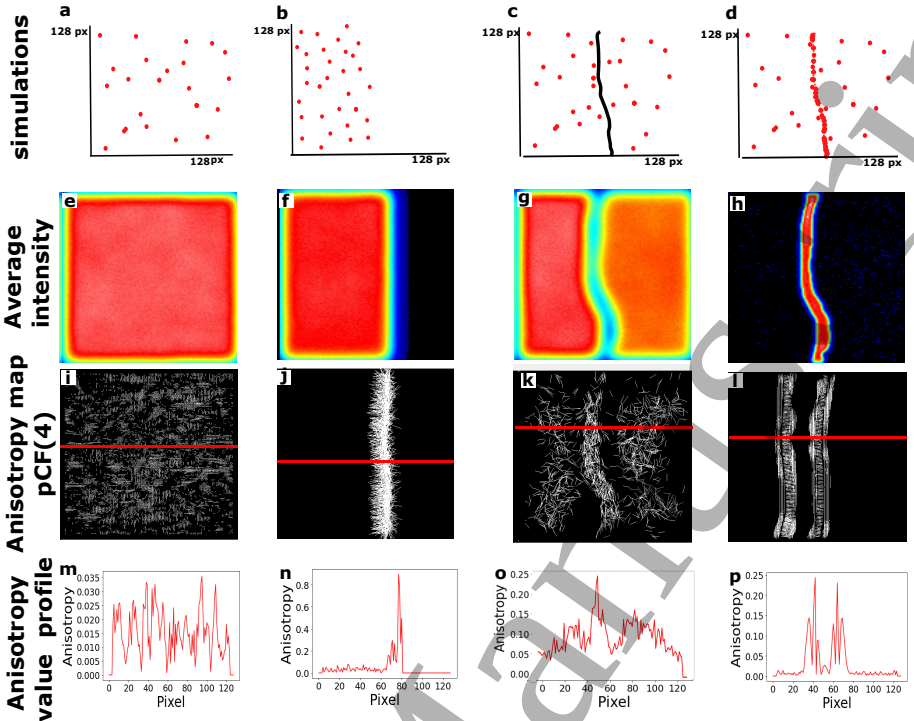


Fig. 2. **The anisotropy value maps highlight the presence of barriers to diffusion**. The 2D pair correlation analysis was applied to simulated data for four cases. Molecules undergoing (a) isotropic diffusion in a free space (b) isotropic diffusion in the presence of an impenetrable barrier (c) isotropic diffusion on both sides of an impenetrable barrier (d) and in the presence of a permeable barrier with a 2 pixels width. The first row (a-d) shows schematic representations of the simulation. On the second row (e-g), the average intensity is presented. In panels h to l the 2D anisotropy map computed at 4 pixels is shown. The red line identifies the position where the anisotropy profile (m-p) was computed. Analyzing the peaks of anisotropy we can determine that when there isn't any peak we have an isotropic diffusion (m); when there is only one we have an impenetrable barrier to diffusion (n and o) and if there is more than one peak we can detect that molecules are translocated through the barrier (p).

### *2.3. Cell Culture*

As previously described by Torrado [23] and Tedeschi [24], NIH/3T3 (ATCC) cells were cultured in Dulbecco's modified Eagle medium (Life) supplemented with 10% v/v fetal bovine serum (FBS, Life), and 1% v/v Penicillin/Streptomycin Solution 100X (10,000 units of penicillin and 10 mg/mL streptomycin in 0.85% saline solution, GenClone, Genesee) at 37°C in a 5% CO2 incubator. For the mEGFP control, we added to the medium, 3 $\mu$l/ml of Hygromycin to encourage the expression of mEGFP. Cells were transfected with GAP-mEGFP plasmid (pCAG-mEGFP was a gift from Connie Cepko, Addgene plasmid #14, 757; RRID: Addgene 14757). One day before transfection, cells were seeded in 35 mm glass bottom dishes (MatTek Corporation). Transfections were performed with Lipofectamine 3000 Kit (Invitrogen, TermoFisher Scientific ) diluted in Opti-MEM I reduced-serum medium (Gibco, TermoFisher Scientific) and a P3000 buffer according to manufacturer instructions. Approximately one day after transfection, Opti-MEM medium was substituted with culture medium (Dulbecco's modified Eagle medium supplemented with 10% v/v Fetal Bovine and 1% v/v Penicillin/Streptomycin Solution 100X). Cells were maintained

in the incubator (37 °C and 5% CO2) before fluorescence microscopy experiments (24 hs after transfection).

### *2.4. Confocal microscopy*

For laser scanning confocal microscopy experiments, images were acquired with an LSM 880 inverted microscope (Zeiss) and a Plan/Apochromat 63x/1.4 oil-immersion objective (Zeiss). The pixel time was set at 3 $\mu$s, the pixel size was 160 nm, and the images had 128x128 pixels corresponding to an area of 20.5 x 20.5 $\mu$m. We have acquired 8000 frames (frame time 120 ms) for each measurement. All experiments were carried out using a detection pinhole size of 1 Airy unit. During the experiment duration, cells were kept at 37°C in a 5% CO2 temperature-controlled chamber. The excitation wavelength was set at 488 nm using an Argon-ion laser and excitation intensities were chosen to achieve a high photon count rate per molecule to maximize the signal/noise ratio but low enough to prevent molecular photobleaching higher than 10% and phototoxicity processes. The obtained photon count rates per molecule ranged from $1x10^6$ cps to $3x10^6$ cps approximately. Fluorescence emission was collected between 498−600nm using a spectral filter and the detection was performed by a GaAsp detector (Hamamatsu) in photon counting mode. Data were analyzed using the commercial software SimFCS (LFD, UCI, www.lfd.uci.edu) and custom-made routines written in Python.

## 3. Results and discussion

### *3.1. Simulations*

While pair correlation analysis has proved to be a powerful technique to investigate the presence of barriers and obstacles to the diffusion of intracellular molecules, its performance has been mainly used to measure transport times and determine intracellular architecture [11, 16, 17, 21]. In this work we will introduce a new capability of the 2D pair correlation analysis using the quantitative measure of the anisotropy as a tool to investigate protein-membrane interactions.

In our simulations there is a barrier to diffusion in the middle of the image. Molecules free diffusing far from the barrier will not be influenced by its presence and their motion can be well characterized by a round SPRITE profile (~zero anisotropy) as expected for isotropic diffusion. However, as the barrier gets closer, the round SPRITE profile becomes distorted in the direction of the barrier thus increasing the anisotropy value, but also indicating the position and orientation of the barrier. Based on this, in each pixel where the obtained SPRITE resulted in an elongated shape (anisotropy ≠ 0), we can infer the position of the barrier and visualize it by drawing a line parallel to the anisotropy direction to build an anisotropy map. To simplify the visualization of the anisotropy map avoiding filling up with many segments in all possible directions, we plot a segment only if the anisotropy value is above a given threshold thus highlighting only the regions with high anisotropy. In conclusion, the presence of a barrier to diffusion causes a preferential direction of transport and an increase in the anisotropy value which can be easily visualized from the anisotropy map.

As a first approach to studying protein-membrane interactions, we'll model the interaction as a decrease in the diffusion coefficient while proteins cross a penetrable membrane schematized by the simulated mask.

#### 3.1.1. Diffusion in the presence of a permeable mask

The most straightforward parameters to model a protein-membrane interaction are controlling the molecular diffusion coefficient (both inside and outside of the mask) and the probability of jumping between regions. In this section, we will consider the latter. We want to explore if there is any dependency in the gap in anisotropy around the membrane with the probability of entering the mask (p). We analyzed a set of simulations that shared all parameters except p which

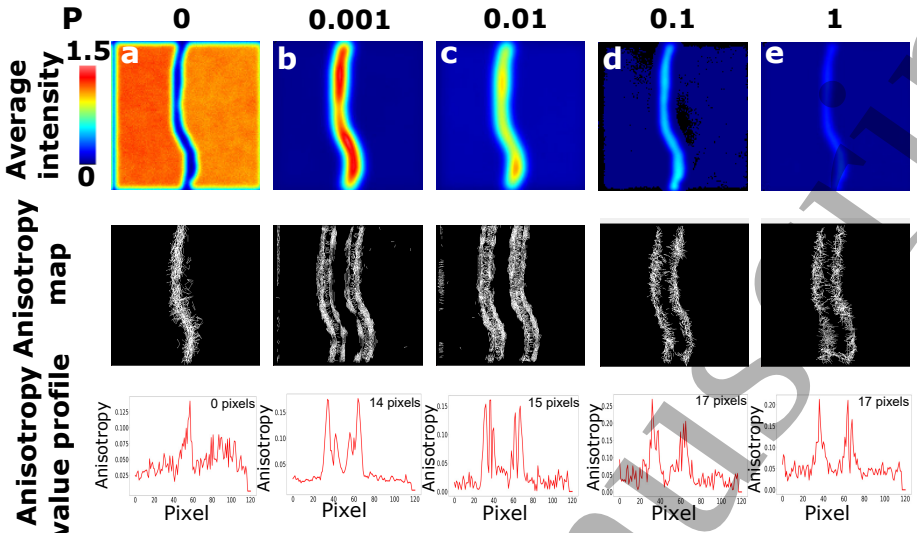


Fig. 3. **The probability of entering and exiting the mask does not affect the gap size**. 2D-pCF(4) analysis was applied to four simulated cases with an increasing probability of crossing the mask. In all simulations molecules diffuse with a $D_{out} = 1\mu m^2/s$ outside the mask and $D_{in} = 0.01\mu m^2/s$. The probability of going through the mask was set from 0 (a) to 1 (e). The first row shows the average intensity of the simulated images. In the second one, the anisotropy maps and a profile of anisotropy (including the gap size) are shown. The threshold of anisotropy was set accordingly to the average anisotropy for each case.

ranged from 0 to 1. In Figure 3 we present the results of the 2D-pCF analysis. The case of p=0 is equivalent to an obstacle to molecular mobility as was described by Malacrida [12]. We can detect the membrane with this analysis and compare it to the simulations with $p > 0$. The results are fundamentally different. For 3(b-e) there is a channel (we will call it gap) in the anisotropy map between the two rows of high anisotropy in the middle of the box, where the mask was set. This gap is not found for p=0.

Additionally simulations (data not shown) revealed that considering a case where particles are present inside the channel with zero probability to cross the barrier, the anisotropy value profile has only one peak and a similar value to the case where there aren't any particles inside the mask (Figure 3a).

The concentration of molecules inside the mask depends on the probability p, being denser as the probability gets smaller which means that it is less probable to exit the mask once a molecule gets inside. Nevertheless, for all the $p > 0$ the size of the gap in anisotropy stayed around the same size (in section 3.1.4 we will show a quantitative analysis on what fluctuations on the gap size we considered significant or not). Then, the probability of entering and exiting a mask (or membrane) is not crucial in determining the size of the gap in the anisotropy.

### 3.1.2. Different diffusion coefficients

So far we have shown results for molecules diffusing at D=$1\mu m^2/s$ outside of the mask. To test the consistency of our results across a broad range of D values we repeated the simulations for different $D_{out}$ in a range from 1 to 40 $\mu m^2/s$. The results presented in Figure 4 illustrate that the size of the anisotropy gap is not solely determined by the molecular diffusion coefficient. It is important to highlight that the anisotropy values actually increase as the diffusion coefficient (D) increases. However, this increase is a consequence of the raster scan detection method utilized in

our simulations, which aims to emulate our experimental setup (refer to Supplementary Material for a comparison between raster scanning detection and camera detection). Importantly, this effect does not have any impact on the size of the anisotropy gap and, as a result, does not affect our presented analysis.

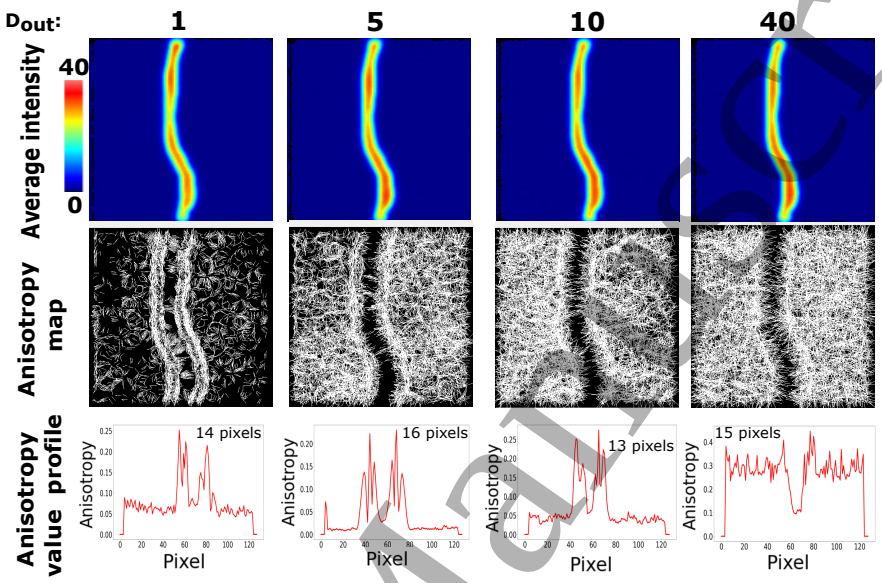


Fig. 4. **The absolute value of the diffusion coefficient does not affect the gap size**. 2D-pCF(4) analysis for simulations where the molecules diffuse outside the mask with D ranging from 1 to 40 $\mu m^2/s$ and p=0.01. The diffusion coefficient inside the mask is set 100 times slower than the outside for each case (ratio=0.01). On the top row, we have the average intensity and on the second row the anisotropy map. The anisotropy threshold is set at the average anisotropy for each simulation. The intensity scale is set from 0 to 40 average photons per pixel. The last row presents a profile of anisotropy for each case including the size in pixels of the resulting gap.

### 3.1.3. Concentration factor

Another factor that may affect the anisotropy maps, is the molecular concentration. We performed simulations with a fixed p=0.01, $Din/D_{out}$ = 0.01, and varying the molecular concentration from 100 to 2000 molecules in the simulated box ( 2 to 50 molecules/$\mu m^2$). Figure 5 shows the results of the 2D pCF analysis. At higher concentrations, the anisotropy outside the mask is lower. This is due to the fact that in those cases at each pixel, we are averaging more molecules resulting in a lower anisotropy (each molecule diffuses freely, if we average enough molecules, there will be no preferential direction). With the anisotropy map, we measure the distance between the two inside walls of high anisotropy around the mask, finding that the gap that shows us the mask has the same size for every concentration.

### 3.1.4. Closing the gap: different ratios of diffusion

Given that we are simulating a membrane by changing the diffusion coefficient inside the mask, the relation between the diffusion inside and outside is a key parameter. In this section, we will focus on how the diffusion coefficient inside the region of the mask ($D_{in}$) affects the molecular flow in their vicinity. In Figure 6 we show the results from the 2D-pCF analysis of simulations

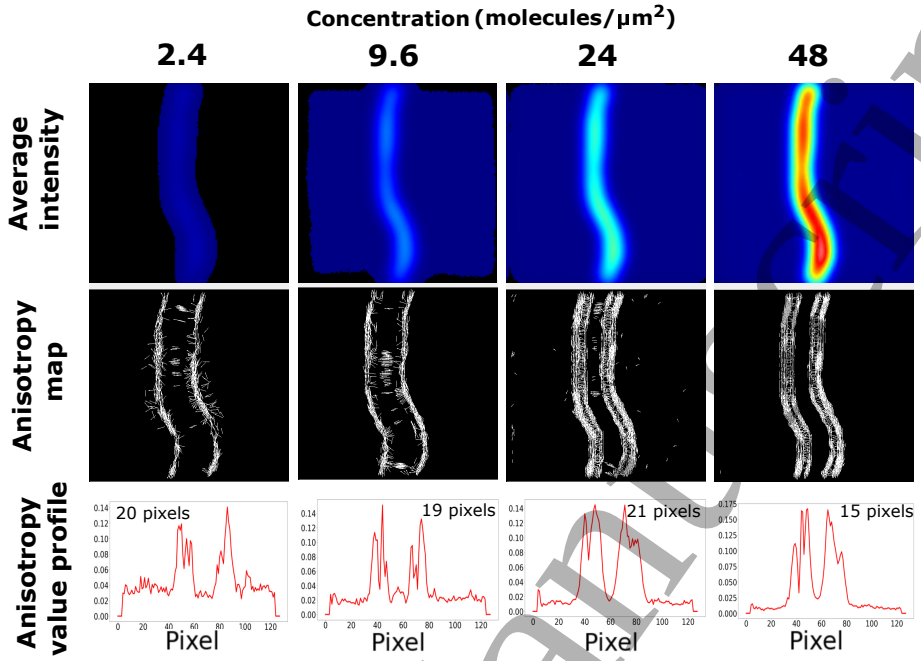


Fig. 5. **The concentration of particles does not affect the size of the gap**. Here we show the 2D-pCF(4) analysis of four simulations where the molecules diffuse outside the mask with D=1 $\mu m^2/s$ and D=0.01 $\mu m^2/s$ inside. The probability of entering/exiting the mask is 0.01 and we changed the concentration of molecules between each simulation. Each column shows the resulting average intensity and anisotropy map for each case, including an anisotropy profile with the size of the gap. It's clear that the gap in the anisotropy map does not change its size with the concentration.

considering a small probability of entering and exiting the mask (p=0.001) and varying the diffusion coefficient ratio ($\frac{D_{in}}{D_{out}}$) from 0.001 ($D_{in} \ll D_{out}$) to 1 ($D_{in} = D_{out}$).

Figures 6 shows the average intensity, and anisotropy value map of the simulated data as a function of $\frac{D_{in}}{D_{out}}$ ratio. The obtained average intensity images, figures 6(a)-(d), show that at smaller ratios, there is a higher concentration of molecules in the region inside the mask. This was expected since, with a low probability of exiting the mask the molecules that diffuse slower inside, will spend on average more time inside the mask than outside. On the other extreme, if the diffusion coefficient is the same inside and out (Ratio = 1) even though the probability (p) remains the same, we don't see the mask with the intensity alone.

As we showed in the Methods section, in the case of Ratio=1, the 2D-pCF analysis highlights the mask which was invisible in the intensity image. Comparing the obtained anisotropy maps between the performed simulations in Figure 6, there are substantial differences among them. There is a gap around the membrane, growing progressively in size and dependent on the ratio of simulated diffusion coefficients. In the anisotropy map, we see a flow of molecules moving at each side of each wall of the mask. These flows get closer to each other as the ratio of diffusion increases, closing the gap. We will say then that if there is a difference in the diffusion inside/outside the mask, we get a gap in the anisotropy map.

For a quantitative analysis of the gap in the anisotropy map, we measure the size of this gap for each case. The results agree with the qualitative analysis of the anisotropy map and are shown in Figure 7: the bigger the difference between $D_{in}$ and $D_{out}$ (smaller ratio) the bigger the gap in

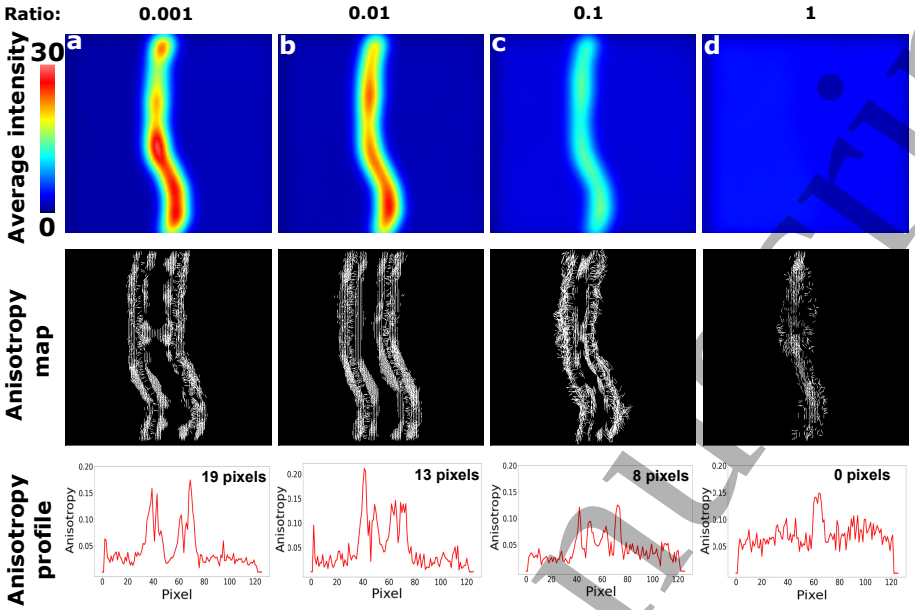


Fig. 6. **The ratio of diffusion coefficients inside/outside the mask determines the size of the gap**. 2D-pCF(4) analysis of four simulations where the molecules diffuse with a fixed D= $1\mu m^2/s$ outside the mask and a fixed probability of entering/exiting of 0.001. The diffusion coefficient inside the mask is set at (a) D=0.001 $\mu m^2/s$, (b) D=0.01 $\mu m^2/s$, (c) D=0.1 $\mu m^2/s$, (d) D=1 $\mu m^2/s$ resulting in ratios ranging from 0.001 ($D_{in}$ 1000 times slower than $D_{out}$) to 1 ($D_{in} = D_{out}$). On the top row, we have the average intensity, on the center row the map of anisotropy. The anisotropy threshold is set at 0.06 for all of them. On the bottom row a profile of anisotropy is included with the corresponding size of the gap (in pixels).

the anisotropy map around the mask. When applying this to cells, where the mask would be a membrane, we consider that a smaller ratio could be linked to a stronger interaction between the molecules we are studying and the membrane. This way, we could apply 2D-pCF to recognize the interaction strength (IS) between protein membranes.

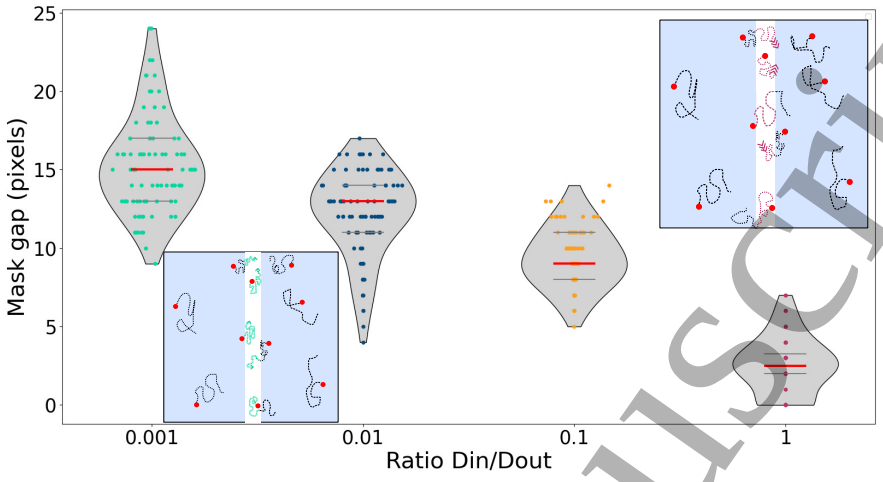


Fig. 7. **The median gap size in the anisotropy map decreases as the diffusion coefficient ratio increases**. Violin plots of the size of the gap extracted from the anisotropy map for different ratios $D_{in}/D_{out}$. The red line indicates the median and the gray lines the 25th and 75th percentiles. For each condition, ten independent repetitions of the simulations were included and ten line scans were analyzed resulting in N = 100 data points per condition. Embedded there are two schemes of the box simulated. One where around the mask the molecules diffuse slower (lower-left), another where they diffuse like outside of it (upper-right).

### *3.2. Experiment validation*

As an experimental verification of our capacity to detect the interaction stregth between protein and membranes, we performed a 2D-pCF analysis on cells transfected with GAP-mEGFP. This construct is the membrane-bound form of mEGFP and as is not functional, its diffusion is only dictated by the surrounding environment [24]. We could expect GAP-mEGFP to have a greater anisotropy gap around the plasmatic membrane compared to that of mEGFP. In Figure 8 we show the results of our 2D-pCF analysis on this system. We corroborated the membrane affinity of GAP-mEGFP by observing the intensity images (left panels). While the concentration of mEGFP is homogeneous in the cell interior, the concentration of GAP-mEGFP is higher close to the plasmatic membrane as indicated by warmer colors in the intensity images. The obtained anisotropy maps show other differences. Even if the diffusion of both proteins shows an increase in the anisotropy direction colocalizing with the membrane position, the GAP-mEGFP protein exhibits a gap in the anisotropy map that is absent for the monomeric form corroborating our hypothesis.

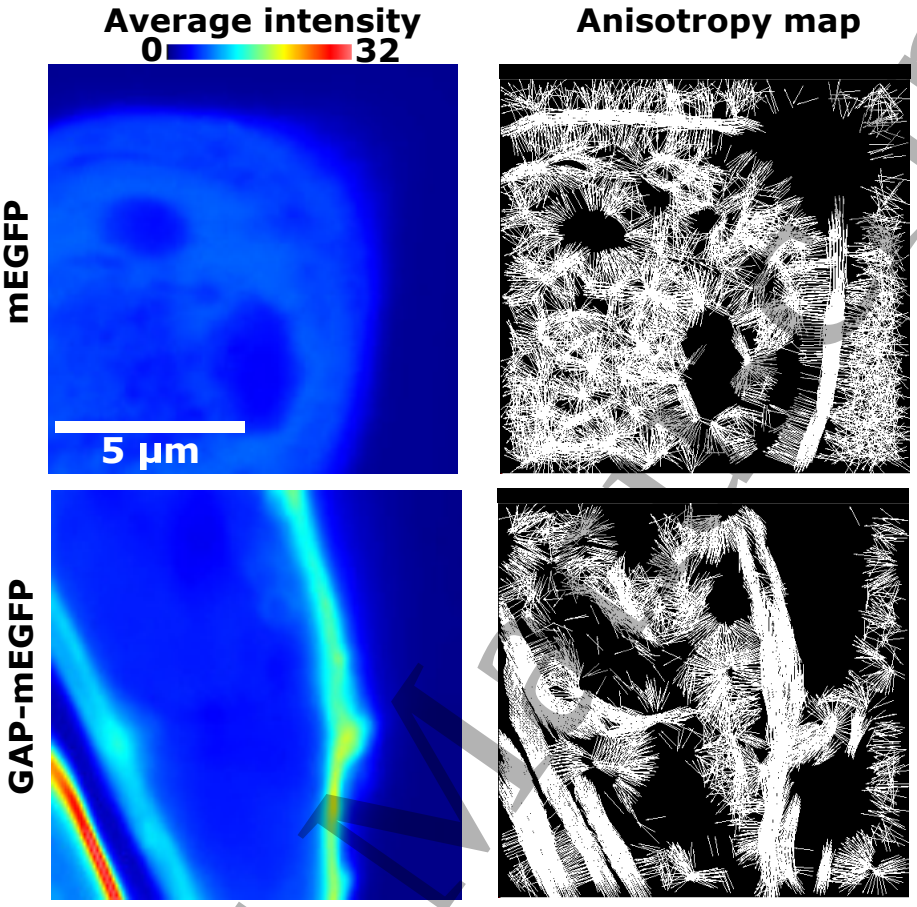


Fig. 8. **The membrane-bound form of mEGFP (GAP-mEGFP) shows differences in the intensity and anisotropy images**. 2D-pCF(4) analysis of the free mEGFP (top row) and the bound-membrane form GAP-mEGFP (lower row). We show the average intensity (left) and the anisotropy map (right) with an anisotropy threshold of 0.2 which corresponds to the average anisotropy of mEGFP (every pixel with anisotropy below that level would be black in the map). The intensity scale is set from 0 to 32 average photons per pixel.

GAP-mEGFP binds to the cell's membrane so there would be a significant proportion of the protein that will be located close to it. This causes that in the membrane vicinity the anisotropy value drops (those already there move without a clear direction) below the chosen threshold for drawing (see Methods) resulting in a gap in the anisotropy map. We calculated the anisotropy gap size for GAP-mEGFP and the control. As it is illustrated in Figure 9, the results are consistent for all our experiments.

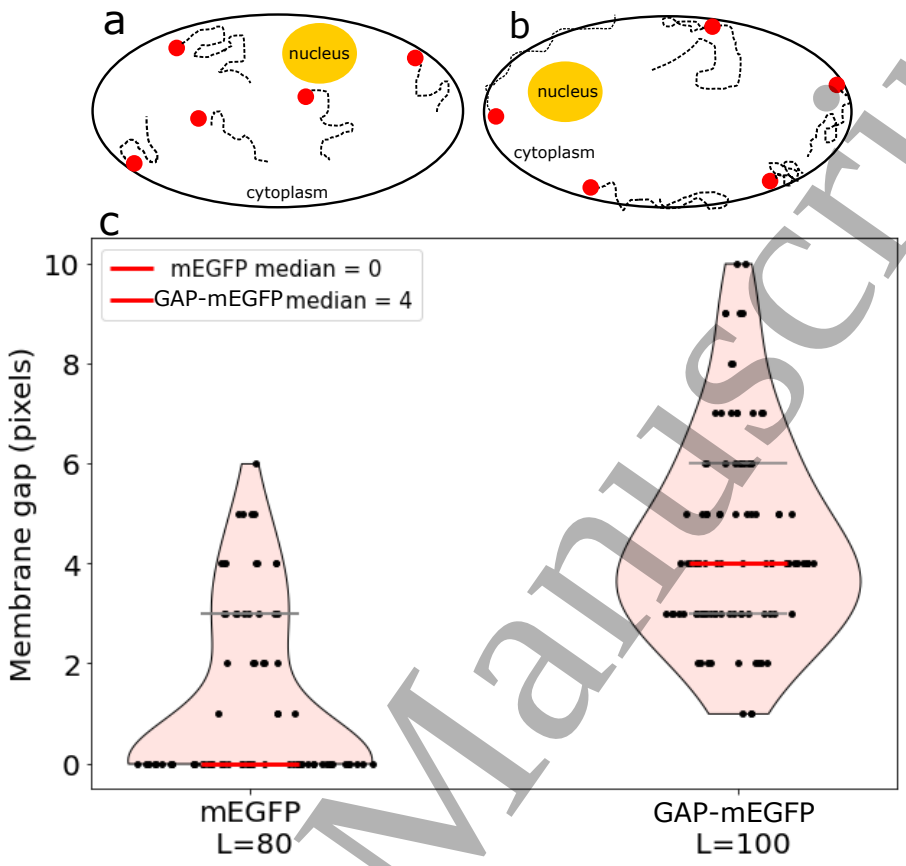


Fig. 9. **The membrane-bound form of mEGFP (GAP-mEGFP) increases the gap size obtained in the anisotropy value map**. The cellular barriers of the plasma membrane were examined and data were acquired in cells transfected with mEGFP or GAP-mGFP. We outline each case: the one with molecules with isotropic diffusion in the cell (a) and the one where there is a preference for diffusing close to the membrane (b). (c): Violin plots of the size of the gap extracted from the anisotropy map. The red line indicates the median and the gray lines the 25th and 75th percentiles. For each condition, eight and ten cells from two independent experiments on two different days were analyzed. In each cell, ten line scans were acquired resulting in L = 80 and L = 100 line measurements respectively.

## 4. Conclusions

Here we demonstrated that the protein-membrane interaction stregth (IS) can be determined by radially correlating intensity fluctuations across pixels in the image. Because the existence of barriers to diffusion inside the cell is mandatory to regulate processes and functions that must take place in different regions of the cell interior, non-invasive techniques capable of visualizing intracellular barriers are necessary to obtain a comprehensive picture of protein interactions that ultimately defined their functions. By simulating data varying molecular concentration, diffusion coefficients, and the probability for the molecules to cross the barriers, we gained insights into the experimental parameters that could modify the obtained anisotropy map of diffusion.

First, we established that either the molecular concentration or the probability to cross the barrier has no incidence in the obtained gap on the anisotropy map. However, we found that as

the ratio of diffusion coefficients across the simulated mask decreases (the molecular mobility becomes similar in and out of the mask) the size of the anisotropy gap disappears. We used the reduction of the diffusion coefficient as a simulation of the IS between the protein and membrane.

Second, cells transfected with a membrane-bound form of the EGFP enlarged the gap size compared with transfection with mEGFP. These results corroborate that the proteins which are designed to efficiently interact with the cell membranes exhibit a larger gap in the anisotropy map.

In conclusion, we demonstrated that the 2D pair correlation approach is a novel method not only for visualizing intracellular barriers to diffusion but also to measure through the anisotropy the degree of protein-membrane interactions opening a new scope of applications to this technique.

## 5. Backmatter

**Funding.**

This work was supported by the Universidad of Buenos Aires grants PIDAE 2020-3980, 2019-3444, Sistema Nacional de Láseres RESOL-2016-42-E-APN-SECACT#MCT and ANPCyT PICT 2020-02718. L.C.E is a member of CONICET. N.P. is currently a Ph.D. fellow from CONICET.

**Acknowledgments.**

We are grateful to Belen Torrado, Gulia Tedeschi, and Balam Benitez-Mara from the Laboratory for Fluorescence Dynamics (LFD) UCI for supplying us with the NIH-3T3 cells, the transfection and assisting us with the cell culture during our experiments.

**Disclosures.** The authors declare no conflicts of interest.

**Data Availability Statement.**

Data underlying the results presented in this paper are not publicly available at this time but may be obtained from the authors upon reasonable request.

**Gender Balance Statement.** While citing references scientifically relevant to this work, we actively worked to promote gender balance. In our reference list, 50% of the cited works correspond to articles where the first and/or corresponding authors have a female first name.

## References

1. C. Eggeling, C. Ringemann, R. Medda, G. Schwarzmann, K. Sandhoff, S. Polyakova, V. N. Belov, B. Hein, C. V. Middendorff, A. Schönle, and S. W. Hell, "Direct observation of the nanoscale dynamics of membrane lipids in a living cell," Nature **457**, 1159–1162 (2009).
2. J. E. Purvis and G. Lahav, "Encoding and decoding cellular information through signaling dynamics," Cell **152**, 945–956 (2013).
3. C. D. Rienzo, E. Gratton, F. Beltram, and F. Cardarelli, "Fast spatiotemporal correlation spectroscopy to determine protein lateral diffusion laws in live cell membranes," Proc. National Acad. Sci. United States Am. **110**, 12307–12312 (2013).
4. C. D. Rienzo, V. Piazza, E. Gratton, F. Beltram, and F. Cardarelli, "Probing short-range protein brownian motion in the cytoplasm of living cells," Nat. Commun. **5** (2014).
5. C. D. Rienzo, F. Cardarelli, M. D. Luca, F. Beltram, and E. Gratton, "Diffusion tensor analysis by two-dimensional pair correlation of fluorescence fluctuations in cells," Biophys. J. **111**, 841–851 (2016).
6. J. M. Kalappurakkal, P. Sil, and S. Mayor, "Toward a new picture of the living plasma membrane," Protein Sci. **29**, 1355–1365 (2020).
7. M. L. Kraft, "Plasma membrane organization and function: Moving past lipid rafts," Mol. Biol. Cell **24**, 2765–2768 (2013).
8. F. J. Alenghat and D. E. Golan, "Membrane protein dynamics and functional implications in mammalian cells," Curr. Top. Membr. **72**, 89–120 (2013).
9. C. Billaudeau, S. Mailfert, T. Trombik, N. Bertaux, V. Rouger, Y. Hamon, H. T. He, and D. Marguet, "Probing the plasma membrane organization in living cells by spot variation fluorescence correlation spectroscopy," Methods Enzymol. **519**, 277–302 (2013).
10. M. Bezanilla, A. S. Gladfelter, D. R. Kovar, and W. L. Lee, "Cytoskeletal dynamics: A view from the membrane," J. Cell Biol. **209**, 329–337 (2015).
11. M. A. Digman and E. Gratton, "Imaging barriers to diffusion by pair correlation functions," Biophys. J. **97**, 665–673 (2009).

12. L. Malacrida, P. N. Hedde, S. Ranjit, F. Cardarelli, and E. Gratton, "Visualization of barriers and obstacles to molecular diffusion in live cells by spatial pair-cross-correlation in two dimensions," Biomed. Opt. Express **9**, 303 (2018).
13. K. Bacia, E. Haustein, and P. Schwille, "Fluorescence correlation spectroscopy: Principles and applications," Cold Spring Harb. Protoc. **2014**, 709–725 (2014).
14. M. A. Digman and E. Gratton, "Lessons in fluctuation correlation spectroscopy," Annu. Rev. Phys. Chem. **62**, 645–668 (2011).
15. M. A. Digman, "Functional role of membrane lipids in egf receptor dynamics and regulation," Cell Membr. Nanodomains: From Biochem. to Nanoscopy pp. 41–58 (2014). Fluctuation spectroscopy methods for the analysis of membrane processes. In <i>Cell Membrane Nanodomains: From Biochemistry to Nanoscopy, UC Irvine.
16. M. Gabriel, G. S. Navarro, L. de Borba, A. H. Rossi, A. V. Gamarnik, and L. C. Estrada, "Dengue virus capsid protein dynamics reveals spatially heterogeneous motion in live-infected-cells," Sci. Reports **10**, 1–13 (2020).
17. I. Sallaberry, A. Luszczak, N. Philipp, G. S. Navarro, M. V. Gabriel, E. Gratton, A. V. Gamarnik, and L. C. Estrada, "In vivo pair correlation microscopy reveals dengue virus capsid protein nucleocytoplasmic bidirectional movement in mammalian infected cells," Sci. Reports **11** (2021).
18. F. G. C. Tedesco, P. S. Aguilar, and L. C. Estrada, "Correlation analyses reveal differential diffusion behavior of eisosomal proteins between mother and daughter cells," Methods Appl. Fluoresc. **10**, 044012 (2022).
19. F. Cardarelli, "Time-resolved biophysical approaches to nucleocytoplasmic transport," Comput. Struct. Biotechnol. J. **15**, 299–306 (2017).
20. M. Baum, F. Erdel, M. Wachsmuth, and K. Rippe, "Retrieving the intracellular topology from multi-scale protein mobility mapping in living cells," Nat. Commun. **5** (2014).
21. E. Hinde, F. Cardarelli, M. A. Digman, and E. Gratton, "In vivo pair correlation analysis of egfp intranuclear diffusion reveals dna-dependent molecular flow," Proc. National Acad. Sci. United States Am. **107**, 16560–16565 (2010).
22. E. Hinde, F. Cardarelli, M. A. Digman, and E. Gratton, "Changes in chromatin compaction during the cell cycle revealed by micrometer-scale measurement of molecular flow in the nucleus," Biophys. J. **102**, 691–697 (2012).
23. B. Torrado, M. Graña, J. L. Badano, and F. Irigoín, "Ciliary entry of the hedgehog transcriptional activator gli2 is mediated by the nuclear import machinery but differs from nuclear transport in being imp-/1-independent," PLoS ONE **11** (2016).
24. G. Tedeschi, L. Scipioni, M. Papanikolaou, G. W. Abbott, and M. A. Digman, "Fluorescence fluctuation spectroscopy enables quantification of potassium channel subunit dynamics and stoichiometry," Sci. Reports **11** (2021).